Molecular dynamics study on low-energy sputtering properties of MgO surfaces

Hyo-Shin Ahn,[1] Tae-Eun Kim,[1] Eunae Cho,[1] Miran Ji,[1] Choong-Ki Lee,[1] Seungwu Han,[1,a)] Youngmi Cho,[2] and Changwook Kim[2]
[1]*Department of Physics, Ewha Womans University, Seoul 120-750, Republic of Korea*
[2]*CAE team, Samsung SDI, Co., Ltd., Yongin 446-557, Republic of Korea*

(Received 30 July 2007; accepted 28 January 2008; published online 9 April 2008)

In an effort to understand microscopic processes occurring between MgO protective layers and impinging plasma ions in a discharge cell of plasma-display panel, sputtering properties of MgO(100) surface by He, Ne, and Xe atoms are studied with molecular dynamics simulations. Interatomic potentials between constituent atoms are fitted to first-principles data sets for representative configurations. Various incident directions of ions are considered with kinetic energies under 100 eV. It is found that sputtering yields for the Ne atom are largest among tested noble gases. The angle dependence of sputtering yields indicates that (111)-oriented MgO films are much more vulnerable to ion attacks than (100)-oriented layers. A surface model including the monolayer step is also studied and it is found that the yields increase substantially for grazing-angle incidence. © *2008 American Institute of Physics*. [DOI: 10.1063/1.2899182]

I. INTRODUCTION

Magnesium oxide (MgO) is known to be a material suitable for many technological applications such as templates for crystal growth, catalysts or optical devices. The chemical, electrical, and mechanical inertness of MgO also enabled its use as a coating layer for various purposes. In particular, the MgO thin film has become an essential part in plasma-display panel (PDP) to protect underlying dielectric materials from energetic plasma ions in sheath region and thereby extend the lifetime of PDP.[1] It also emits secondary electrons to sustain plasma ions and lower the operation voltage.[2] Although MgO is known for its high sputter resistance, a lifetime-limiting factor in PDP is still the erosion of the protective layer due to ion-surface interactions. Therefore, for the continual development of PDP, it is important to understand the sputtering property of MgO, in particular, its dependence on ion species and surface conditions. In fact, there have been many efforts to improve the device performance and lifetime of PDP by optimizing growth directions and surface morphologies of MgO.[3–5]

From Monte Carlo simulations on ions and neutrals in plasma gases, it has been known that most of inert gases in discharge cells impinge on the MgO surface with kinetic energies below 100 eV.[6,7] Experimentally, the surface-charging makes it difficult to study surface-ion interactions at such low kinetic energies. On the theoretical sides, the ability to describe atomic processes of the momentum and energy transfer is required for investigating low-energy collisions. In this respect, statistical approaches based on Monte Carlo methods[7] are rather approximate, and simulations at the level of first-principles or classical molecular dynamics (MD) are appropriate tools to investigate the sputtering behavior of MgO in PDP. Since a full-blown first-principles simulation of sputtering is still beyond most of current computational capabilities, the classical MD simulation seems to be the method of choice at the present time. In Ref. 8, MD simulations were performed on the sputtering of MgO surfaces to explain texture evolutions during ion-beam-assisted deposition (IBAD). (Note that the kinetic energy in that work was typically several hundred electronvolts.)

The interaction potentials used in classical MD simulations are usually obtained through a fit to reference values for bulk phases such as lattice parameters, cohesive energies, and elastic constants. Therefore, the fitted potentials are most suitable for the simulation of a system close to the crystalline phase. When studying ion-surface interactions, however, one needs to modify parameters to reflect changes in chemical environments. Due to the dearth of experimental data in those systems compared to bulk phases, first-principles results are useful as a reference data set. For example, first-principles results on energy barriers in surface diffusion or electron populations in small clusters were applied to fitting interatomic potentials for MgO.[8–10] On the other hand, repulsive interactions between noble gases and surface ions such as Mg or O atoms have not been carefully examined as far as we are aware. In this work, based on first-principles results for representative configurations, we select or fit interatomic potentials to be employed in simulating plasma gases impinging on MgO surfaces in PDP. Using the developed potentials, we carry out MD simulations on the sputtering yields of the MgO (100) surface by He, Ne, and Xe atoms and investigate their dependence on various conditions of projectiles and surfaces.

II. COMPUTATIONAL METHODS

For the classical MD simulations to evaluate sputtering yields, we employ the LAMMPS code, a MD simulation package available in public domain.[11] The interactions between Mg–Mg, Mg–O, and O–O atoms are described by ionic pair

a)Author to whom correspondence should be addressed. Electronic mail: hansw@ewha.ac.kr.

potentials, so-called the Buckingham potential, suggested by Lewis and Catlow.[12] This potential consists of the long-range Coulomb interaction, short-range repulsive part, and long-range van der Waals interactions as formulated below

$$V_{\alpha\beta}(r) = \frac{Z_\alpha Z_\beta e^2}{r} + A_{\alpha\beta}\exp\left(\frac{-r}{\rho_{\alpha\beta}}\right) - \frac{C_{\alpha\beta}}{r^6}, \quad (1)$$

where r is a separation between ions α and β with atomic number Z, and $A_{\alpha\beta}$, $\rho_{\alpha\beta}$, and $C_{\alpha\beta}$ are fitting parameters. Various choices of parameters will be compared in the next section. For evaluating long-range Coulomb interactions, particle-per-particle-mesh methods are used.[13]

On the other hand, the interactions between O-X and Mg-X ions, where X indicates one of He, Ne, and Xe atoms, are described by a functional form suggested by Molière,[14]

$$V(r) = \frac{Z_\alpha Z_\beta e^2}{r}\left[0.35\exp\left(-\frac{0.3r}{a}\right) + 0.55\exp\left(-\frac{1.2r}{a}\right) + 0.1\exp\left(-\frac{6.0r}{a}\right)\right], \quad (2)$$

where a is a screening parameter. This potential is essentially a sum of screened Coulomb potentials. Boers[15] proposed that a is equal to $ca_0(Z_\alpha^{1/2}+Z_\beta^{1/2})^{-2/3}$, where c is a fitting parameter and a_0 is the Bohr radius. The Firsov screening lengths are obtained with $c=1$.[16] In this work, we use c as a fitting parameter (see below). For comparison, the universal potential developed by Ziegler *et al.* is also examined.[17] Ziegler–Biersack–Littmark (ZBL) potential is similar to Eq. (2) except for the number of terms and parameter values as shown in the following:

$$V(r) = \frac{Z_\alpha Z_\beta e^2}{r}\left[0.1818\exp\left(-\frac{3.2r}{a}\right) + 0.5099\exp\left(-\frac{0.9423r}{a}\right) + 0.2802\exp\left(-\frac{0.4029r}{a}\right) + 0.02817\exp\left(-\frac{0.2016r}{a}\right)\right], \quad (3)$$

where the screening parameter a is $0.8853a_0(Z_\alpha^{0.23}+Z_\beta^{0.23})^{-1}$.

For first-principles calculations of selected reference geometries, Vienna *Ab Initio* Simulation Package (VASP) is used.[18] The ionic potentials are described by projector-augmented-wave methods[19] and exchange-correlation energies of electrons are described within the generalized gradient approximation.[20] The energy cutoff of 400 eV is used to generate a plane-wave basis set. The lattice constant of bulk MgO is computed to be 4.238 Å in comparison with the experimental value of 4.211 Å. We use a $2\sqrt{2}\times 2\sqrt{2}$ unit cell of (100) surface within periodic boundary conditions. A slab model including ten layers of MgO is used with a vacuum length of 10 Å. For the k-point integration, we use a $2\times 2\times 1$ mesh for the unit supercell of MgO surface. In order to confirm that bulk properties are recovered in the middle of the slab, we examine two structural parameters; interlayer spacing and anion-cation buckling distance for each layer. The results are summarized in Table I and it is seen that the structural parameters well converge to bulk values from the third layer. (In the case of the interlayer spacing, all data agree with the bulk value within the computational accuracy.) In addition, we examine partial density of states projected on each layer. As shown in Fig. 1, surface states are confined within two layers from the surface and bulklike densities of states develop from the third layer. Therefore, it is concluded that the model with ten layers is thick enough to recover bulk properties in the middle region.

TABLE I. Interlayer distances between layers i and $i+1$ and anion-cation buckling distances for each layer of the model MgO slab. The layer 1 means the top surface. Units are in angstroms.

Layer	Interlayer distance (Å)	Anion-cation buckling (Å)
1	2.121	0.051
2	2.120	0.007
3	2.119	0.002
4	2.115	0.000
5	2.113	0.001
6	2.115	0.001
7	2.119	0.000
8	2.120	0.002
9	2.121	0.007
10		0.051
Bulk	2.119	0.000

III. SELECTION OF POTENTIAL PARAMETERS

A. Buckingham potential

We first choose a parameter set for the Buckingham potential. For studying sputtering properties, detachment of at-

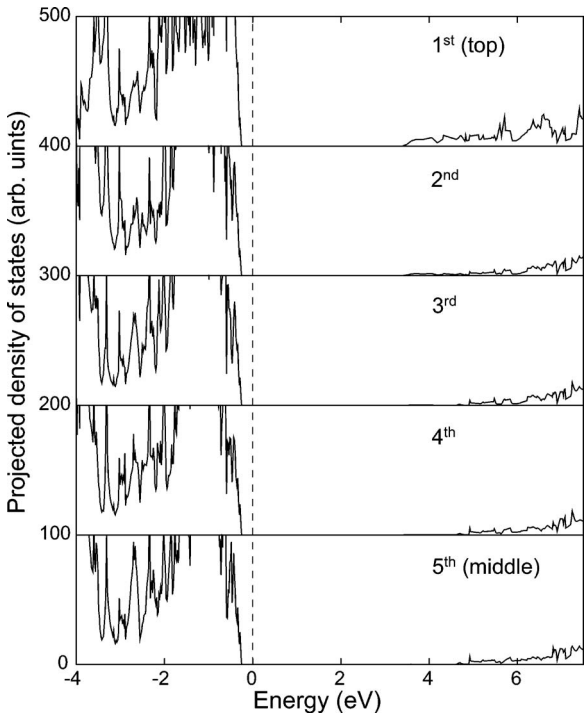

FIG. 1. The density of states projected on each layer in the model MgO slab.

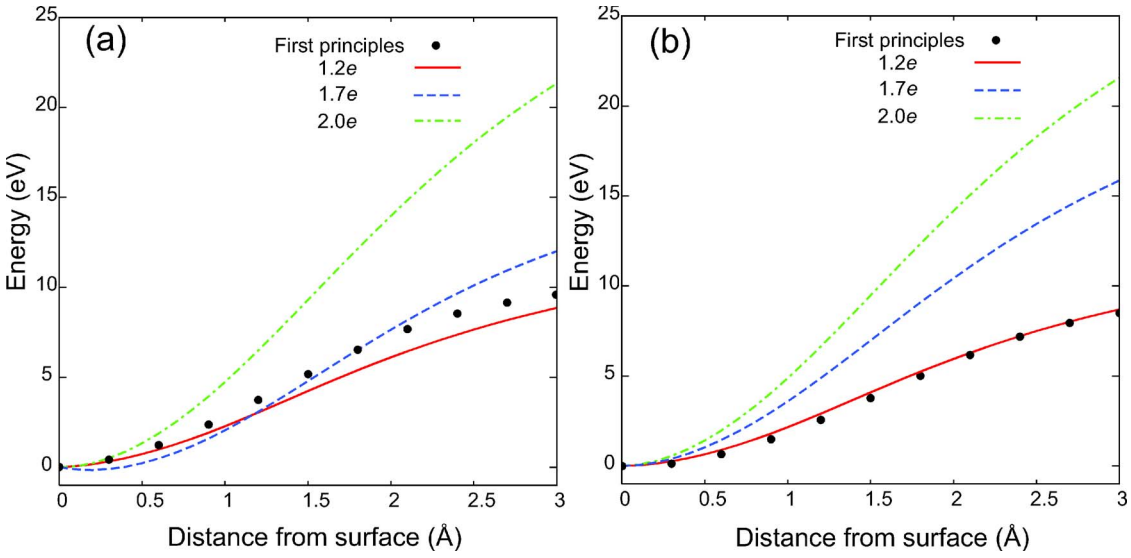

FIG. 2. (Color online) The energy curves with respect to the distance of (a) O or (b) Mg atoms from the surface as they are detached from the original position at 0 Å.

oms from the surface is a central process. For reference configurations used as first-principles inputs, Mg or O atoms are separated from the clean (100) surface without any relaxation. The distances between detached atoms and the surface are varied from 0 Å (the equilibrium position) up to 3 Å. Three parameter sets for the Buckingham potential are compared, each of them adopted from Refs. 8–10, respectively. The major differences between parameter sets are charge states of Mg and O atoms. In Ref. 8, the nominal charge ($\pm 2.0e$) of the ionic crystal is used. The analysis of electron population based on the Bader method has shown that partial charges are close to $\pm 1.7e$.[9] Using these charge values, better agreements between first-principles and empirical results were achieved for migration energies of surface adatoms. On the other hand, from the population analysis of MgO clusters, Kubo *et al.* found that $\pm 1.2e$ is appropriate when describing undercoordinated atoms.[10] Other bulk properties such as lattice parameters and elastic constants are well addressed by all parameter sets.

Figure 2 compares first-principles data with empirical results using three parameter sets in the above. It is found that the slope of the energy curve by classical potentials is well correlated with the magnitude of partial charges. This means that the Coulomb interaction between detached ions and charged surfaces largely determines the energy profile in empirical potentials. The comparison with first-principles results indicates that the best fits are obtained for both Mg and O detachments when partial charges of $\pm 1.2e$ are used. Other parameters result in significant over-binding. The ionic charges of $\pm 1.2e$ was obtained with small MgO clusters as reference configurations.[10] The low coordination numbers for sputtered atoms should be better described by this model. The potential parameters adopted from Ref. 10 are summarized in Table II.

B. Adjusted Molière potential

Next, we try to fit potentials to describe repulsive interactions between noble gases and Mg or O atoms. For noble gases, we choose He, Ne, and Xe atoms which are main components of the plasma gas in PDP discharge cells. The potential curves at small separations between incident ions and surface atoms dictate energy and momentum transfers during atomic collisions. In order to obtain the reference profile, the total energies are calculated using first-principles methods with noble gases fixed on top of Mg or O atoms. The vertical distances between ions and underlying surface atoms are varied between 1 and 3 Å. All atoms are fixed to their equilibrium positions. To estimate accuracies of existing interatomic potentials, energies for the same configurations are evaluated with the ZBL potentials [Eq. (3)] applied to Mg-X and O-X pairs (X=He, Ne, and Xe). The results are shown in Fig. 3 with comparison to first-principles data. Overall, the agreements at separations between 1 and 3 Å are surprisingly good considering the level of approximations employed in ZBL potentials. However, energy curves are rather overestimated when He and Ne atoms approach from the above of Mg atoms. This is attributable to electron transfers between Mg and O atoms; although the atomic number of magnesium is higher than that of oxygen, electron transfers to O atoms may result in less repulsive interactions for Mg atoms.

To improve the agreement of classical potentials and first-principles data, we employ Molière potential [Eq. (2)] and optimize c in screening parameters for Mg-X and O-X pairs (X=He, Ne, and Xe) by fitting to first-principles values. We add that results with the original Molière potential (c =1) greatly overestimate energy curves. It is also noted that the energy curve is the sum of repulsive interactions between

TABLE II. Parameters for the Buckingham potentials.

	$A_{\alpha\beta}$ (eV)	$C_{\alpha\beta}$ (eVÅ^6)	$\rho_{\alpha\beta}$ (Å)
Mg–Mg	3943	0	0.16
Mg–O	63613	0	0.165
O–O	872060	0	0.17

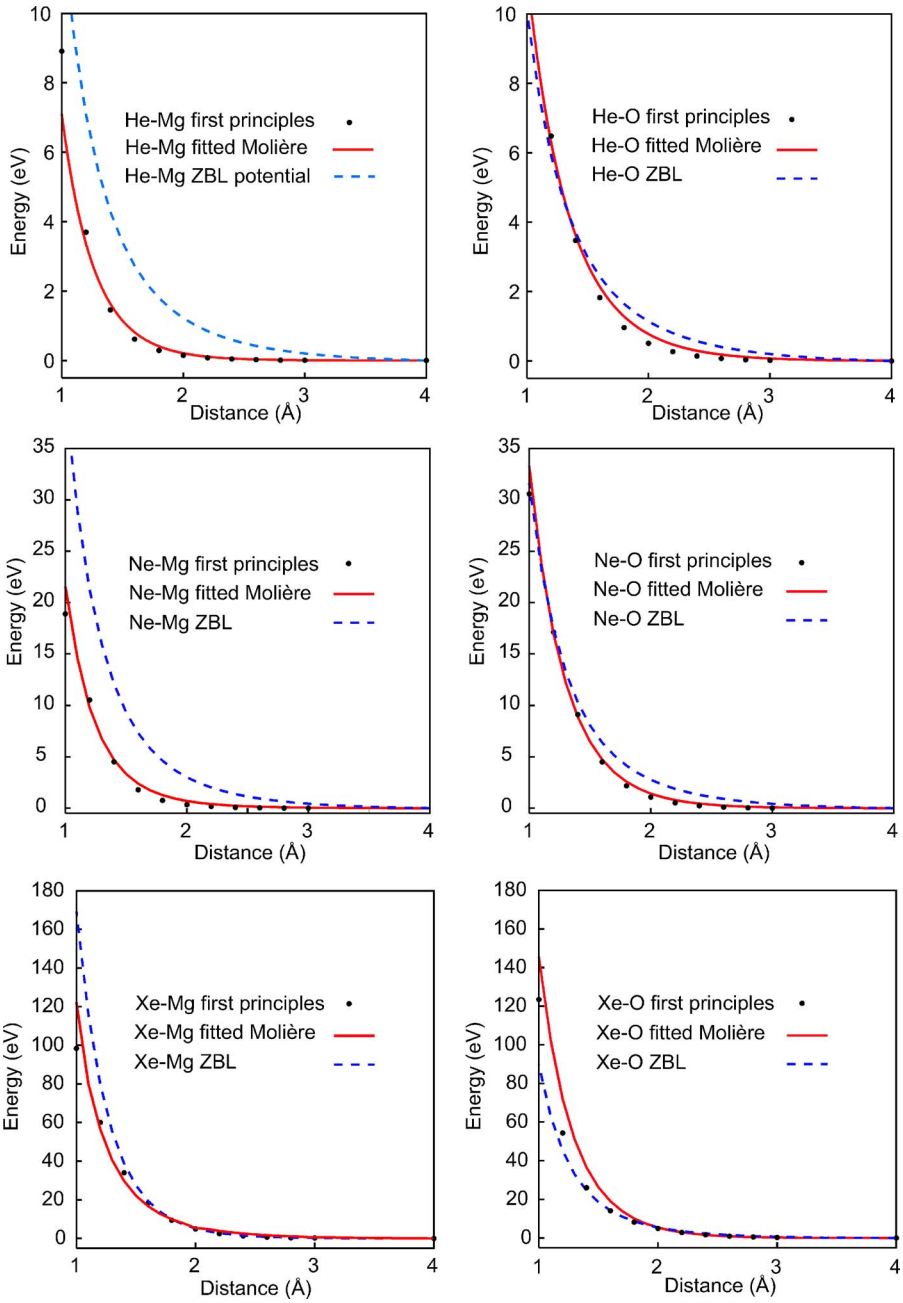

FIG. 3. (Color online) Energy curves with respect to the distance between ions and surface atoms (magnesium or oxygen). The reference values calculated with first-principles methods are shown as dots and the results by empirical potentials are drawn with dashed (ZBL) or solid lines (fitted Molière).

several pairs around impact points, rather than a single contribution by the closest Mg-X or O-X pairs. The results obtained with optimized parameters are shown in Fig. 3 and fitted parameters are compiled in Table III. While interactions between Xe and surface atoms are well described by the Firsov screening length, those involving He and Ne atoms show significant departures from $c=1$. In other words, the original Molière potential would overestimate repulsive interaction and hence underestimate sputtering yields especially for low-energy collisions.

TABLE III. The fitted screening parameters (c) for the Molière potentials.

	He	Ne	Xe
Mg ion	0.65	0.66	1.046
O ion	0.80	0.84	1.07

IV. RESULTS AND DISCUSSION

A. Model system and computational setup

To study low-energy sputtering properties of MgO surfaces, we carry out classical MD simulations with the empirical potentials developed in the previous section. As a model substrate, we choose $6\times6\times5$ MgO lattice sites with the clean (100) surface exposed to the vacuum. [See Fig. 4(a).] Periodic boundary conditions are imposed in the lateral dimensions. To prevent any drift of the substrate after ionic bombardments, atoms in the bottom layer are fixed throughout the simulation. The initial temperature of the MgO substrate is set to 300 K since PDP operates on ambient conditions.[21] MD simulations are carried out on constant energy surfaces.

In choosing collision angle θ which is the angle between the incident direction and surface normal (see Fig. 4), we

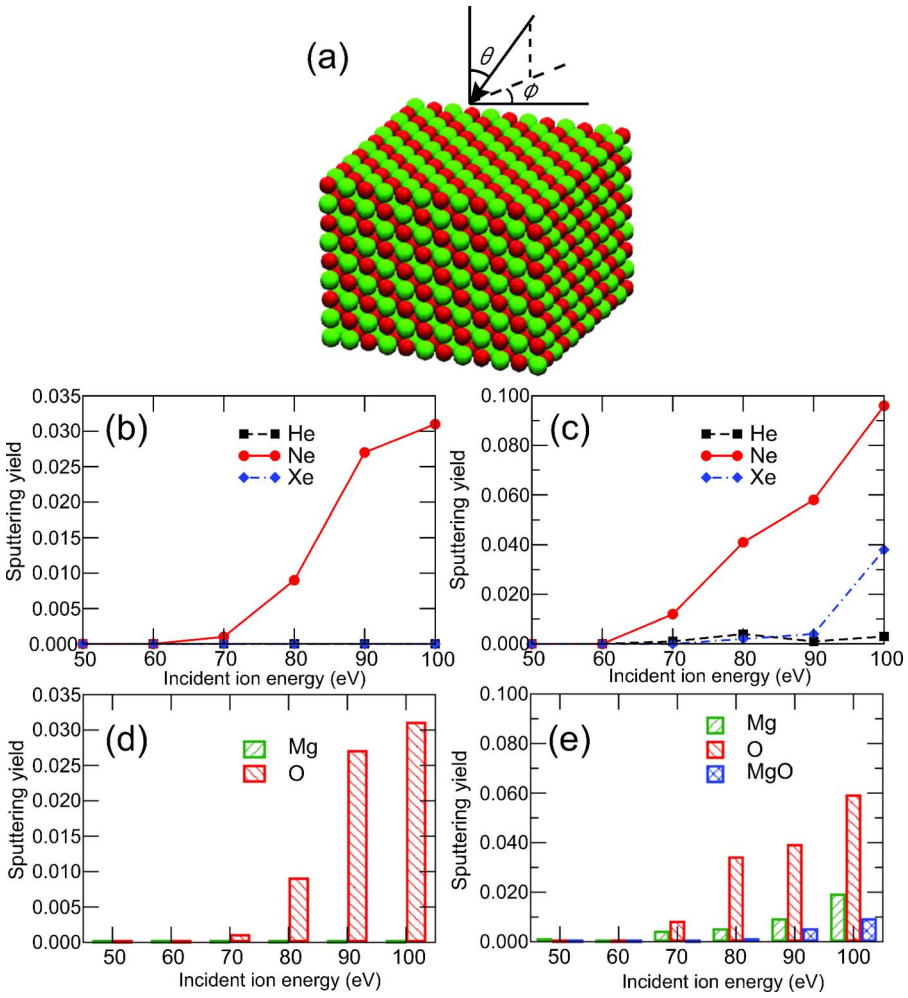

FIG. 4. (Color online) (a) The model system to calculate the sputtering yields. Sputtering yields with respect to the ion species and incident energies are shown in (b) and (c) for $\theta=0°$ and $\theta=54.7°$, respectively. [See (a) for the definition of θ.] The distributions of sputtered types for the collision with Ne atoms are shown in (d) and (e) for $\theta=0°$ and $\theta=54.7°$, respectively.

consider preferential growth directions of MgO thin films. The protective layer in PDP is usually grown with e-beam evaporation or ion-plating methods. Depending on various growth conditions, MgO thin films show preferred orientations along the (100) or (111) crystallographic directions.[22–24] In both cases, the surfaces are always faceted with stable (100) surfaces. On the other hand, most of plasma ions are incident on the surface from the direction normal to electrodes. Combining these two factors, it is concluded that ionic impingements on (111)-oriented MgO films are equivalent to the incidence on (100) surface from $\theta=54.7°$. For the (100)-oriented films, θ is simply zero. Furthermore, while the out-of-plane texture is well developed along the (100) or (111) orientations, the in-plane texture of the thin film is randomly oriented. This means that the azimuthal angle of incident directions should be averaged in the simulations.

The sputtering rate per incident atom is evaluated by counting the number of sputtered atoms (except for the projectile atom) after 2 ps simulations. For statistical sampling, 1000 independent runs are carried out with random impact points and azimuthal angles (see above) of incident projectiles. An atom is considered as sputtered if it is separated from the substrate by more than 7 Å at the end of the simulation. In order to confirm that redeposition on the surface does not occur, we extend the simulation time to 4 ps for all runs showing finite yields and make it sure that the detached atoms or molecules still satisfy the sputtering criterion. The incident kinetic energies are varied up to 100 eV which is the maximum kinetic energy for plasma ions with meaningful populations.[6,7]

Due to the finite thickness and periodic boundary conditions, the phonons generated by incident ions reflect from the bottom or propagate to neighboring cells, and it should be confirmed that they do not affect the computational results significantly. To this end, we carry out a test calculation on a larger supercell made of $10\times10\times8$ lattice sites. As a projectile, we choose the Ne atom incident along the $\langle111\rangle$ direction with the kinetic energy of 100 eV, which results in the highest sputtering yield in our simulations (see below). The resulting sputtering rate for $10\times10\times8$ supercell is larger than that for $6\times6\times5$ supercell by 5%. This amount of increase in sputtering yields does not affect conclusions drawn in this work.

B. Sputtering rates for the (100) and (111) orientations

Figure 4 shows computed sputtering rates for $\theta=0°$ and 54.7° corresponding to collisions to MgO surfaces with the (100) and (111) growth directions, respectively. It is notable that the sputtering yields for $\theta=54.7°$ incidence is substantially larger than those for $\theta=0°$. In the latter case, the pri-

TABLE IV. Comparison of sputtering rates with previous results.

Ion	Energy (eV)	This work		Empirical extrapolation[a]	Monte Carlo[b]
		$\theta=0°$	$\theta=54.7°$		
He	80	0.000	0.004	···	0.083
He	90	0.000	0.001	···	0.090
He	100	0.000	0.003	···	0.100
Ne	80	0.009	0.041	0.010	0.105
Ne	90	0.027	0.058	0.024	0.119
Ne	100	0.031	0.090	0.040	0.129
Xe	80	0.000	0.002	0.007	0.000
Xe	90	0.000	0.004	0.013	0.000
Xe	100	0.000	0.038	0.024	0.000

[a]Reference 6.
[b]Reference 7.

mary knock-on atom moves deep into the substrate and subsequent collisions lead to a momentum transfer mostly in the downward direction, which does not contribute to sputtering yields. A similar angle dependence of sputtering yield was reported in Ref. 8 for higher kinetic energies. It is also noticeable in Fig. 4 that the yields are largest for Ne atoms. This can be understood based on the classical two-body collision, where the largest momentum transfer occurs when masses are the same. Among He, Ne, and Xe atoms considered in the simulation, Ne atom ($Z=10$) has an atomic mass most similar to those of oxygen ($Z=8$) or magnesium ($Z=12$) atoms. On the other hand, He atoms hardly sputter out surface atoms. Due to a small atomic size, the collisional cross section for the He atom is much smaller than those of Ne or Xe atoms. As a result, He atoms mostly penetrate into the substrate rather than transferring energies to the lattice. For Xe atoms, we find that they often shift knock-on atoms to other areas in the surface without affecting the sputtering yield. This implies that Xe atoms in the PDP cell could substantially modify surface morphologies of MgO films by means of the mass transport. We also inspect differential distributions of sputtered atoms for Ne atoms in Figs. 4(d) and 4(e). It is found that most of sputtered atoms are oxygen. The larger size of oxygen atoms should be a primary reason. At higher energies, Mg atoms or MgO molecules begin to be identified. On the other hand, it is found that Xe atoms sputter out predominantly MgO molecules over the whole range of incident energies (not shown in the figure). The large atomic size of Xe is more effective in transferring the momentum to MgO molecular units as a whole.

In Table IV, we compare the computed sputtering yields with previous results in Refs. 6 and 7. Since the surface directions were not specified in those works, it is difficult to draw a direct comparison. Furthermore, our results are for the perfect surface and therefore should be considered as lower bounds, while the previous estimations might have considered defective surfaces in an average sense. Overall, estimations in Refs. 6 and 7 are similar to one of the results for $\theta=0°$ and $\theta=54.7°$. However, our sputtering yields for the Xe atom are substantially smaller compared to Ref. 6 at low-energy regions. On the other hand, the sputtering rate of the He atom seems to be overestimated in Ref. 7. The information on the cross section in Ref. 7 might have not addressed the chemical environments of the ionic crystal such as charge transfers between anions and cations.

Based on the calculated sputtering yield of each species, one can roughly estimate the lifetime of the MgO films. Following a simplified procedure used in Ref. 7, we assume that the lifetime is equivalent to the time span needed to remove the whole thickness of MgO films purely through the damage by plasma ions. We adopt physical parameters from Ref. 7 such as distributions of kinetic energies of ions, film thickness or gas pressures, except for the sputtering rate for which we use the estimation obtained by MD simulations. The calculated lifetime for $\theta=0°$ is larger than for $\theta=54.7°$ by several orders over a wide range of gas pressures and compositions. This strongly implies that the (111)-oriented MgO films are vulnerable to attacks by plasma ions and has a negative effect on the lifetime of PDP.

C. Angle-dependent sputtering rates

In order to understand further the low-energy sputtering characteristics of the MgO surface, we investigate the sputtering yields for Ne and Xe atoms with respect to various incident angles. The computational results are shown in Fig. 5. Regardless of incident energies or ionic species, the sputtering yields are peaked around 50°. Around this angle, the initial momentum transfer and ensuing cascade events are concerted so as to sputter out atoms most efficiently.

After a collision with surface atoms, the projectile atom can be retained within the MgO matrix or escape into the vacuum, and this would affect the long-term stability of MgO thin films. To obtain information on this, we examine the location of impinging ions at the end of the simulation. An ion staying below the surface layer is counted as retained. Figure 6 shows the retention probability calculated for different angles and ion species when the incident energy is 100 eV. (Some atoms, notably for He, simply go through the whole thickness of the slab and escape out of the bottom layer. In this case, we regard them as being retained.) Following things are noticeable: (i) the smaller ions prefer staying inside the slab. (ii) The capture probability decreases for high incident angles. (iii) The retention probability is peaked at the $\langle 111 \rangle$ direction, indicating channeling effects. From the inspection on impact points, it is also found that when inci-

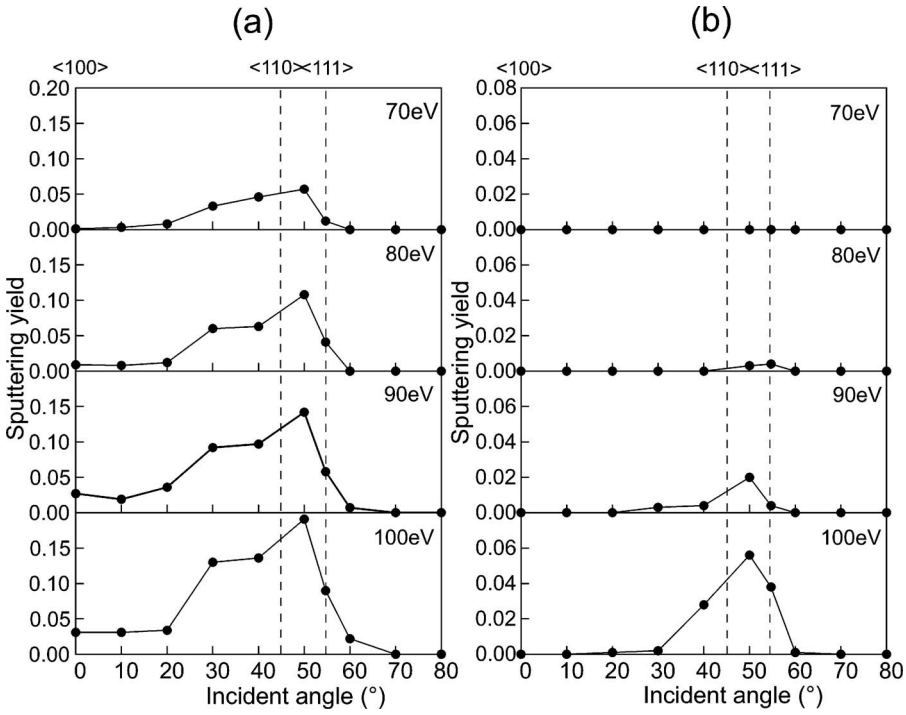

FIG. 5. Sputtering yields with respect to incident energies and angles; (a) Ne and (b) Xe atoms. The vertical dashed lines indicate angles corresponding to representative directions.

dent atoms make a close contact with surface atoms, large portions of the kinetic energy are lost and chances of being retained are significantly reduced. In the case of Xe atoms, it is also observed that the penetration depth is small and the atoms stay just below the surface for most of the simulation time.

In Ref. 8, the lowest sputtering yield for the ⟨110⟩ direction was related to the channeling effects of MgO. Indeed, the above results for the retention probability also peaked at the ⟨111⟩ direction (The ⟨110⟩ direction corresponds to 45° and was not sampled.), implying that channeling effects are also present in these low-energy sputtering simulations. However, the angle-dependent yield curves shown in Fig. 5 do not show noticeable changes around channeling directions. This is attributable to two simulation conditions that are different from Ref. 8, which, in turn, reflects dissimilar experimental situations between IBAD and PDP. Firstly, the results in this work are averaged over azimuthal angles while the simulation in Ref. 8 was for the specific angle (θ=45°, ϕ=0°) corresponding to the ⟨110⟩ direction. Therefore, the channeling effects would be smeared in our simulations as a result of the average over the whole range of azimuthal angles. Secondly, the kinetic energies in our work are much lower than those in Ref. 8 and therefore the penetration depth into the substrate is also smaller. That is to say, even if the ions are incident from the channeling directions, the low kinetic energies result in short traveling distances and therefore the channeling effect is not significant compared to the high-energy impingements in Ref. 8.

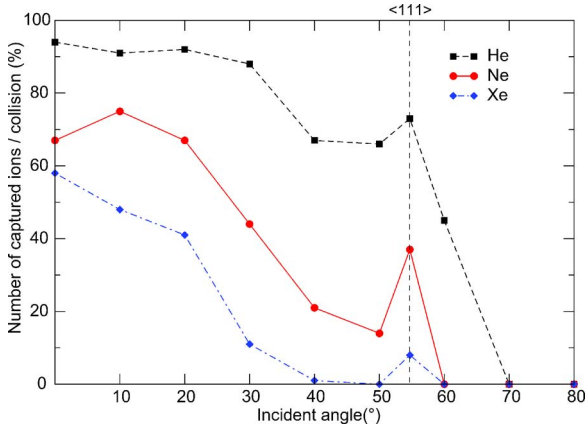

FIG. 6. (Color online) The probability that the impinging ion is captured within the MgO substrate at the end of the 2 ps simulation. The kinetic energy is 100 eV.

D. Sputtering rates for surface steps

As another intriguing application, we study sputtering yields of defective surfaces. During the PDP operation, significant defect densities will develop on the surface of MgO protective layer due to the continual collision with plasma ions. Surface steps will be one of the main defects conceivable for MgO surfaces under this condition. Therefore, we introduce a monolayer step on (100) surface periodically and calculate the sputtering yields when Ne atoms are incident. It is noted that ions impinge on random points in the surface, not specifically along the step edge. As is shown in Fig. 7, the sputtering yields for the step model are significantly different from those for clean surfaces presented in Fig. 5. First, it is observed that the yields are larger at grazing angles ($\theta \sim 70°$). This is certainly due to the weak bonds near the step edge. To be more specific, it is found that the sputtering properties are different depending on whether the ions hit near the step region from upward or downward directions, as described pictorially in Fig. 7(c). For collisions at grazing angles, the momentum transfer is dominated along the directions parallel to the surface. Therefore, when the ion hits on the step from the above ("downward"), the momentum transfer to edge atoms lead to high sputtering probabilities. In

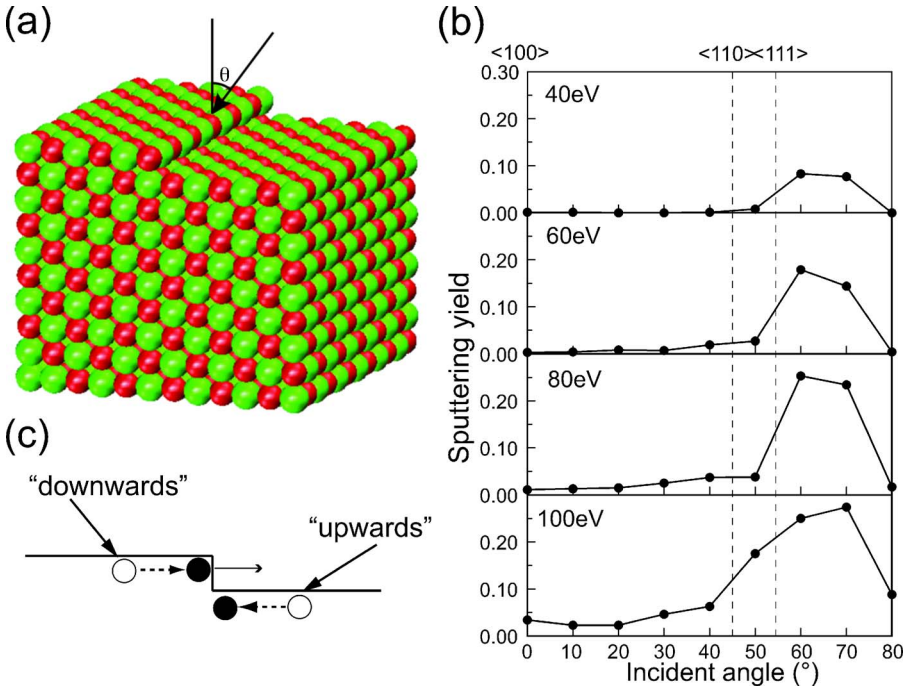

FIG. 7. (Color online) (a) The unit cell of the model structure including the surface step. (b) Sputtering yields for collisions with Ne atoms with respect to the incident energy and angle. (c) Schematic picture explaining the main sputtering mechanism at grazing angles.

fact, this accounts for most of the sputtering events identified. On the other hand, when the ion is incident from the lower terrace ("upward"), the sputtering is blocked by the atoms near the step and the collision does not lead to sputtering as far as we have observed. In addition, for the range of 50°–80°, sputtering yields are rather insensitive to incident energies between 60 and 100 eV. This means that the threshold energy to sputter an edge atom is around 30–40 eV and therefore yields are saturated at higher energies.

It is also notable that the data at 30°–40° is only half of the values for clean surfaces. This is counterintuitive because the clean surface is chemically more stable than defective surfaces. Further analysis shows that most of detached atoms originate from the upper terrace. This is indicative of a shadowing effect; the step structure partially screens the collision with atoms at the lower terrace. This substantially suppresses the sputtering near the step edge. In our model system, the surface steps are repeated with a short period (three unit cells) and therefore computational results are substantially affected by this effect.

V. SUMMARY

In summary, we have developed a parameter set suitable for describing the collision between the MgO surface and discharge gases in PDP. By carrying out molecular dynamics simulations, we calculated the low-energy sputtering yields of MgO. We found that He, Ne, and Xe atoms show distinct sputtering behaviors; the He atom is too small to make an efficient collision, the Ne atom shows the largest yields, and the Xe atom is not an effective sputterer but can induce a large surface modification by moving surface atoms. We believe that our results will be useful to optimize various parameters in the discharge cell of PDP such as gas compositions, gas pressures, and surface orientations of MgO protective layers.

ACKNOWLEDGMENTS

This work was supported by Samsung SDI and the Korea Science and Engineering Foundation through the Basic Research program (Grant No. R01-2006-000-10883-0). The computations were carried out at Korea Institute of Science and Technology Information (KISTI) through the 8th Strategic Supercomputing Program.

[1] H. Uchiike, K. Miura, N. Nakayama, T. Shinoda, and Y. Fukushima, IEEE Trans. Electron Devices **23**, 1211 (1976).
[2] Y. Cho, C. Kim, H.-S. Ahn, E. Cho, T. Kim, and S. Han, J. Appl. Phys. **101**, 083710 (2007).
[3] J.-K. Kim, K.-S. Moon, K.-W. Whang, and J.-H. Lee, J. Vac. Sci. Technol. B **19**, 687 (2001).
[4] Y. H. Cheng, H. Kupfer, F. Richter, H. Giegengack, and W. Hoyer, J. Appl. Phys. **93**, 1422 (2003).
[5] M. J. Lee, S. Y. Park, S. G. Kim, H. J. Kim, S. H. Moon, and J. K. Kim, J. Vac. Sci. Technol. A **23**, 1192 (2005).
[6] L. C. Pitchford, J. Wang, D. Piscitelli, and J. P. Boeuf, IEEE Trans. Plasma Sci. **34**, 351 (2006).
[7] S. J. Yoon and I. Lee, J. Appl. Phys. **91**, 2487 (2002).
[8] L. Dong, L. A. Zepeda-Ruiz, and D. J. Srolovitz, J. Appl. Phys. **89**, 4105 (2001).
[9] G. Henkelman, B. P. Uberuaga, D. J. Harris, J. H. Harding, and N. L. Allan, Phys. Rev. B **72**, 115437 (2005).
[10] M. Kubo, Y. Oumi, R. Miura, A. Fahmi, A. Stirling, A. Miyamoto, M. Kawasaki, M. Yoshimoto, and H. Koinuma, J. Chem. Phys. **107**, 4416 (1997).
[11] S. J. Plimpton, J. Comput. Phys. **117**, 1 (1995); http://lammps.sandia.gov
[12] G. V. Lewis and C. R. A. Catlow, J. Phys. C **18**, 1149 (1985).
[13] R. W. Hockney and J. W. Eastwood, *Computer Simulation Using Particles* (Hilger, New York, 1989).
[14] G. Molière, Z. Naturforsch. A **2**, 133 (1947).
[15] A. L. Boers, Surf. Sci. **63**, 475 (1977).
[16] O. B. Firsov, Sov. Phys. JETP **6**, 534 (1958).
[17] J. F. Ziegler, J. P. Biersack, and U. Littmark, *The Stopping and Range of Ions in Solids* (Pergamon, New York, 1985).
[18] G. Kresse and J. Hafner, Phys. Rev. B **47**, 558(R) (1993); **49**, 14251 (1994).
[19] P. E. Blöchl, Phys. Rev. B **50**, 17953 (1994).
[20] J. P. Perdew, K. Burke, and M. Ernzerhof, Phys. Rev. Lett. **77**, 3865 (1996).

[21]K. Tsutsumi, M. Ishimoto, T. Fukasawa, G. Uchida, H. Kajiyama, and T. Shinoda, Proceedings of the 12th International Display Workshops, IDW'05, Sendai, Japan, 2005 (unpublished), p. 1515.
[22]J.-H. Boo, S.-B. Lee, K.-S. Yu, W. Koh, and Y. Kim, Thin Solid Films **341**, 63 (1999).
[23]J.-G. Yoon, H. K. Oh, and S. J. Lee, Phys. Rev. B **60**, 2839 (1999).
[24]R. Plass, J. Feller, and M. Gajdardziska-Josifovska, Surf. Sci. **414**, 26 (1998).